



In situ investigation of commercial Ni(OH)(2) and LaNi5-based electrodes by neutron powder diffraction

Downloaded from: <https://research.chalmers.se>, 2024-03-20 12:28 UTC

Citation for the original published paper (version of record):

Biendicho, J., Roberts, M., Noreus, D. et al (2015). In situ investigation of commercial Ni(OH)(2) and LaNi5-based electrodes by neutron powder diffraction. *Journal of Materials Research*, 30(3): 407-416. <http://dx.doi.org/10.1557/jmr.2014.317>

N.B. When citing this work, cite the original published paper.

In situ investigation of commercial Ni(OH)₂ and LaNi₅-based electrodes by neutron powder diffraction

Jordi Jacas Biendicho^{a)}

The ISIS Facility, STFC Rutherford Appleton Laboratory, Oxfordshire 11 0QX, United Kingdom; and Department of Materials and Environmental Chemistry, Stockholm University, Stockholm 106 91, Sweden

Matthew Roberts

Department of Materials Chemistry, Ångström Laboratory, Uppsala University, Uppsala 751 21, Sweden

Dag Noréus

Department of Materials and Environmental Chemistry, Stockholm University, Stockholm 106 91, Sweden

Ulrika Lagerqvist

Nilar Svenska AB, Gavle 800 08, Sweden

Ronald I. Smith

The ISIS Facility, STFC Rutherford Appleton Laboratory, Oxfordshire 11 0QX, UK

Gunnar Svensson

Department of Materials and Environmental Chemistry, Stockholm University, Stockholm 106 91, Sweden

Stefan T. Norberg and Sten G. Eriksson

Department of Chemical and Biological Engineering, Chalmers University of Technology, Sweden 412 96, Sweden

Stephen Hull

The ISIS Facility, STFC Rutherford Appleton Laboratory, Oxfordshire 11 0QX, UK

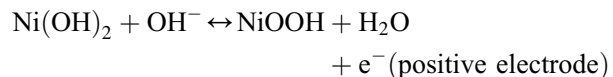
(Received 13 June 2014; accepted 3 October 2014)

Electrochemical reactions at both positive and negative electrodes in a nickel metal hydride (Ni-MH) battery during charge have been investigated by in situ neutron powder diffraction. Commercially available β -Ni(OH)₂ and LaNi₅-based powders were used in this experiment as positive and negative electrodes, respectively. Exchange of hydrogen by deuterium for the β -Ni(OH)₂ electrode was achieved by ex situ cycling of the cell prior to in situ measurements. Neutron diffraction data collected in situ show that the largest amount of deuterium contained at the positive electrode is de-intercalated from the electrode with no phase transformation involved up to ~ 100 mA h/g and, in addition, the 110 peak width for the positive electrode increases on charge. The negative electrode of composition MmNi_{3.6}Al_{0.4}Mn_{0.3}Co_{0.7}, where Mm = Mischmetal, exhibits a phase transformation to an intermediate hydride γ phase first and then to the β phase on charge. Unit cell dimensions and phase fractions have been investigated by Rietveld refinement of the crystal structure.

I. INTRODUCTION

Nickel-metal hydride batteries (Ni-MH) appeared on the market toward the end of the 1980s, replacing other nickel-based rechargeable batteries such as the nickel-cadmium system.¹ In the Ni-MH battery, the hydrogen at the positive electrode is de-intercalated during charge and absorbed at the metal alloy (M) working as a “hydrogen sponge”. The half-cell reactions at the positive and negative electrodes are presented below. The use of metal hydride (MH) material as the anode

increased the storage battery capacity and extended the cycle life with respect to Ni-Cd and Ni-Fe batteries. Ni-MH batteries compete directly with Li-ion batteries even though they have lower energy densities. Applications range from portable electronics to hybrid electric vehicles e.g., the Toyota Prius is powered by a 27 kW Ni-MH battery²



^{a)}Address all correspondence to this author.

e-mail: jordi.jacas@stfc.ac.uk

DOI: 10.1557/jmr.2014.317

Numerous forms of nickel hydroxide and oxy hydroxide exist.^{3,4} Bode⁵ described the reactions taking place at the positive electrode in an alkaline storage battery. The β form of nickel hydroxide, i.e., $\beta\text{-Ni(OH)}_2$, has the CdI₂ type structure with a hexagonal close packing arrangement of the oxygen atoms and Ni²⁺ atoms occupying the octahedral sites. During charge, one proton per formula is extracted from $\beta\text{-Ni(OH)}_2$ and the $\beta\text{-NiOOH}$ phase is formed. In spite of the low crystallinity of the charged phase,⁶ the general understanding of the charge/discharge process is that minor structural changes occur at the electrode i.e., contraction of the *ab*-plane of the unit cell due to shorter Ni–O distances and elongation in the *c* direction due to the increased repulsion between NiO₂ slabs. This isostructural phase transition $\beta_{\text{II}} \leftrightarrow \beta_{\text{III}}$, where II and III refer to nickel oxidation states, was first proposed by Bode⁵ and has been supported by ex situ measurements.^{7,8} More recently, $\beta\text{-NiOOH}$ obtained by chemical oxidation at room temperature was investigated by diffraction techniques and high-resolution electron microscopy (HREM).^{9,10} The structure was different from the originally proposed one by Bode⁵ due to shearing of the NiO₂ layers along the *ab*-plane and it was refined using a monoclinic unit cell with ABCA stacking of the oxygen atoms along the *c* axis. The authors anticipated that this form of $\beta\text{-NiOOH}$ would effectively correspond to an intermediate phase between the discharged $\beta\text{-Ni(OH)}_2$ phase and the $\gamma\text{-NiOOH}_x$ form, the latter being formed when the electrode is over-oxidized⁵ and, therefore, the $\beta_{\text{II}} \leftrightarrow \beta_{\text{III}}$ transition involves severe structural changes.^{11,12} The $\gamma\text{-NiOOH}_x$ form represents a whole family of compounds¹³ characterized by a) poor crystallinity and b) incorporation of water molecules and alkali protons into the structure. Depending on synthesis conditions,¹⁴ different forms of $\gamma\text{-NiOOH}_x$ may be prepared which show larger unit cell dimensions compared to $\beta\text{-Ni(OH)}_2$ and an oxidation state of nickel between 3 and 3.75. The most accepted description of $\gamma\text{-NiOOH}_x$ is a layered structure in which oxygen atoms are stacked in the ABBCCD sequence.^{13,15} Another form of nickel hydroxide that may play a role during electrode charge/discharge is $\alpha\text{-Ni(OH)}_2$ ^{11,16} which, from the structural point of view, is very similar to the $\gamma\text{-NiOOH}_x$ form. Diffraction patterns of $\alpha\text{-Ni(OH)}_2$ show reflections at large *d*-spacings ≥ 8 Å and its structure has been described as turbostratic, i.e., NiO₂ layers have slipped sideways relative to each other. Depending on the electrode preparation and on battery cycling conditions, the redox reaction at the positive electrode may proceed as $\alpha_{\text{II}} \leftrightarrow \gamma_{\text{III}}$ which has shown good reversibility¹⁷ and, more importantly, takes advantage of a large number of electrons exchanged per nickel atom. In summary, the electrochemistry at the positive electrode is rich in terms of observed phases and it is this which has motivated us to investigate commercial electrodes by in situ neutron diffraction in the present paper.

The negative electrode in a Ni-MH battery is a hydrogen storage alloy (MH). Current research focuses on various metallic structures^{18–20} and new preparation methods i.e., surface treatment,²¹ to increase the storage capacity, reduce material production costs, and improve the charge/discharge rate performance of the electrode. For commercial use, LaNi₅-based alloys with the CaCu₅-type structure are preferred. LaNi₅ alloys reversibly intercalate/de-intercalate large amounts of hydrogen and the structure allows multiple cation substitutions on both La and Ni sites which, in turn, can optimize the electrochemical properties of the compound. In the CaCu₅-type structure,^{22–25} there is a stacking of two different planes at *z* = 0 and *z* = 1/2, with the former containing the 1*a* and 2*c* crystallographic sites and the latter the 3*g* sites; lanthanides occupy the 1*a* crystallographic site and transition metals both occupy 2*c* and 3*g* sites. For the charged phase La_xNi_yD_z,²⁶ it was shown that deuterium atoms are mainly located in the 6*m* position, the largest void in the CaCu₅-type structure. The use of in situ diffraction techniques to study phase transitions in intermetallic compounds during charge/discharge has been extensively investigated by Latroche and co-workers^{27–32} and others.^{33,34} The reaction mechanism may vary greatly depending on the alloy composition and electrode cycling conditions. For instance, in MmNi_{4.3-x}Mn_{0.3}Al_{0.4}Co_x (*x* = 0.36 and 0.69)³⁰ where Mm refers to mischmetal, the appearance of an intermediate γ phase was observed for the alloy *x* = 0.69 in addition to the fully charged β phase. For other intermetallic compounds, a typical solid solution behavior has been observed when the alloy is charged, with no phase transition involved i.e., LaNi₄Co.³²

Many electrochemical cells have recently been developed to take advantage of neutron radiation to characterize battery materials.^{35–37} In this paper, our specially designed electrochemical cell²⁶ has been used to investigate the reactions at both electrodes in a Ni-MH battery during charge. To obtain results which may be directly relevant for technological applications, we have used commercially available powders for the experiment. The electrochemistry at the positive electrode is rich in terms of observed phases and still far from being well understood. Due to the higher incoherent scattering section of hydrogen, a detailed structural analysis of hydrogen containing materials is difficult if not impossible. In this paper we show that extended cycling of commercial electrodes containing hydrogen in a deuterated electrolyte, which is continuously exchanged, provides better resolved spectra from which structural information may be extracted. This will improve the understanding of how the present day commercial materials work in real battery electrodes.

II. EXPERIMENTAL

Commercially available positive and negative electrodes were provided by Nilar® and used as received. The AB₅-type alloy in the form of powder was pressed as a pellet using a uniaxial press and the positive electrode pressed into Ni foam to ensure good electrical contact. Both electrodes then were loaded into the electrochemical cell which has been described previously.²⁶ The design of the in situ electrochemical cell is based on the coin-cell geometry and is constructed of a number of circular disk-shaped components. The cell has larger dimensions compared to typical commercial batteries to maximize the amount of electrode material and thus collect diffraction data of good statistical quality within the shortest possible time. An electrochemical cell that maximizes the volume of electrode material exposed to the neutron beam has also been developed by Latrouche.²⁷ To reduce incoherent scattering of hydrogen from typical battery components, a polytetrafluoroethylene (PTFE) separator and 6 M KOD electrolyte were used to construct the battery. The amounts of positive and negative electrodes were 1.2 and 2 g, respectively, and the total capacity of the battery was, therefore, ~230 mA h. Prior to the in situ experiment, the cell was cycled galvanostatically at C/12 between 1–1.5 V for 15 cycles to 1) increase the surface reactivity of the negative alloy and 2) exchange hydrogen by deuterium atoms at the positive electrode to obtain Ni(OD)₂. The capacity retention was ~90% of the theoretical capacity after 15 cycles. The cell was then stopped at the discharged state and dismantled, and the electrodes were carefully washed using heavy water. A new cell was then assembled using a fresh KOD electrolyte for the in situ experiment. In situ neutron diffraction data were collected at the Polaris diffractometer³⁸ in ISIS. The use of the recently upgraded Polaris is motivated by its high incident flux which, in addition to the cell design, allowed neutron diffraction data of good statistical quality to be collected every 30 min. Diffraction data collected in the detector bank at backscattering angles ($135^\circ < 2\theta < 168^\circ$, $d_{\max} = 2.7 \text{ \AA}$, $\Delta d/d = 0.30\%$) were used for Le Bail fit and Rietveld analysis using Fullprof³⁹ and GSAS,⁴⁰ respectively. The Bragg peak profile was described using function 3 (Ref. 40) in GSAS (a convolution of a pseudo-Voigt and two back-to-back exponential functions) and only the components of the Gaussian part of the pseudo-Voigt function refined. The fitting of individual peaks was conducted within the Fullprof software³⁹ using the POLARIS³⁸ instrument file as starting values. The Bragg peak position, its intensity, and the widths of the Gaussian component of the Pseudo-Voigt function in the line shape description were all refined and fits converged. XRD patterns were collected at the Materials Laboratory in ISIS using a Rigaku diffractometer Cu $\alpha 1$ radiation

and simulated diffraction patterns were generated using CrystalMaker.⁴¹

III. RESULTS AND DISCUSSION

X-Ray diffraction (XRD) patterns and scanning electron microscope (SEM) pictures of both positive and negative electrodes are presented in Figs. 1(a) and 1(b), respectively. The XRD pattern of MmNi_{3.6}Al_{0.4}Mn_{0.3}Co_{0.7} where Mm = 50–55% La, 30–35% Ce, 9–13% Nd and 3–5% Pr shows typical reflections corresponding to the CaCu₅-type structure in addition to nickel metal. Reflections were indexed using the hexagonal unit cell in space group *P6/mmm* and refined unit cell dimensions were $a = 5.000(1) \text{ \AA}$, $c = 4.046(3) \text{ \AA}$, and $V = 87.60(5) \text{ \AA}^3$. A SEM micrograph shows alloy particles of size ~100 μm and nickel nanoparticles which ensure good electrical contact between active material particles. Conversely, β -Ni(OH)₂ particles show a well-defined spherical microstructure of diameter <10 μm and the XRD pattern shows broadening of some diffraction lines i.e., 001 and 101. The latter indicates the presence of stacking faults randomly distributed within the

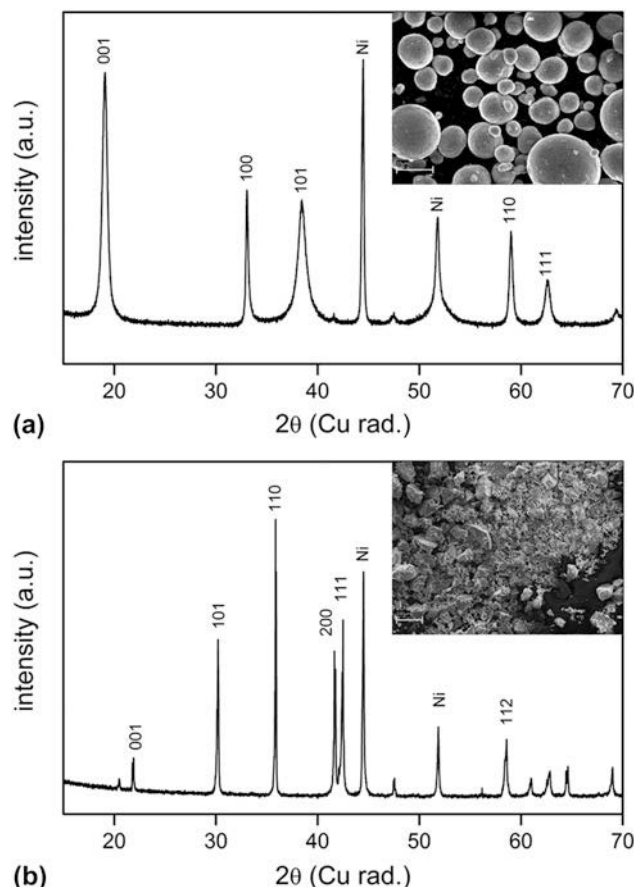


FIG. 1. XRD patterns and SEM pictures of (a) β -Ni(OH)₂ and (b) LaNi₅-type electrode.

hexagonal close packing of the oxygen atoms.⁴² From the line broadening observed in the XRD pattern, Fig. 1(a), and the size of the β -Ni(OH)₂ particles ($<10 \mu\text{m}$) good electrochemical performance is expected as observed in Ref. 43 for a commercial Ni(OH)₂ powder with similar spherical-like particles ($\sim 10 \mu\text{m}$). Indexing of the β -Ni(OH)₂ reflections led to a hexagonal unit cell with lattice parameters $a = 3.126(1) \text{ \AA}$, $c = 4.596(1) \text{ \AA}$, and $V = 38.90(1) \text{ \AA}^3$.

A color contour map showing all the neutron diffraction data collected in situ and battery electrochemistry is presented in Fig. 2. The map shows changes as a function of charge at C/18 ($\sim 12 \text{ mA}$). The voltage versus capacity profile shows the typical behavior for this type of system and nearly full capacity $\sim 190 \text{ mA h/g}$ was achieved before reaching 1.5 V. Neutron diffraction data collected on electrode materials as well as cell components e.g., Ni metal modules, Ni mesh, and Teflon separator were used to identify reflections observed in the neutron diffraction pattern of the cell in the discharged state. Representative patterns of the cell at different charge states and the fit using the above mentioned components as well as other phases that appear in the diffraction patterns as a result of the battery being charged (discussed later) are presented in Fig. 3. The most intense peaks correspond to Ni metal and are due to the cell construction materials. Ni peaks were fitted using the Le Bail method and not considered further. Good agreement between in situ data and structural models was obtained as shown by the goodness-of-fit $\chi^2 \sim 5$.

A. Charge in situ studies of Ni(OD)₂

To identify reflections corresponding to Ni(OD)₂ in the neutron diffraction patterns, simulated diffraction patterns of Ni(OH)₂ and Ni(OD)₂ using neutron radiation are presented in Fig. 4. Both patterns show clear differences in intensity e.g., the 001 peak shows intensity when H is present in the structure but not for Ni(OD)₂. This extinction is due to the positions of the atoms in the crystal structure and the destructive interference originating from Ni, O, and D. The simulated pattern for Ni(OD)₂ shows that the most intense reflections are 101 and 110, which are clearly identified in the neutron diffraction pattern, Fig. 3(a). Notice that the simulated intensity for the 002 reflection is very low compared to 101. At the same time, data collected using bank 3 ($40^\circ < 2\theta < 67^\circ$, $d_{\max} = 7 \text{ \AA}$, $\Delta d/d = 0.86\%$) (not shown) did not show any intensity at d -spacing $\sim 4.6 \text{ \AA}$ for the 001 reflection. On this basis we can assume that hydrogen has been replaced by deuterium during the ex situ experiment, leading to the chemical formula Ni(OD)₂ for the positive electrode. Since only the 110 and 101 reflections were observed in the neutron diffraction pattern of the electrochemical cell, it was decided to monitor the variation of d -spacing, intensity, and full width half maximum (FWHM) as a function of charge state using peak fitting, Fig. 5. Peak maxima for both 101 and 110 in Figs. 6(a) and 6(d), respectively, and also Fig. 2, show a continuous decrease of d -spacing until the intensity of the peaks vanishes into the background. Above $>100 \text{ mA h/g}$, structural information for the positive electrode could

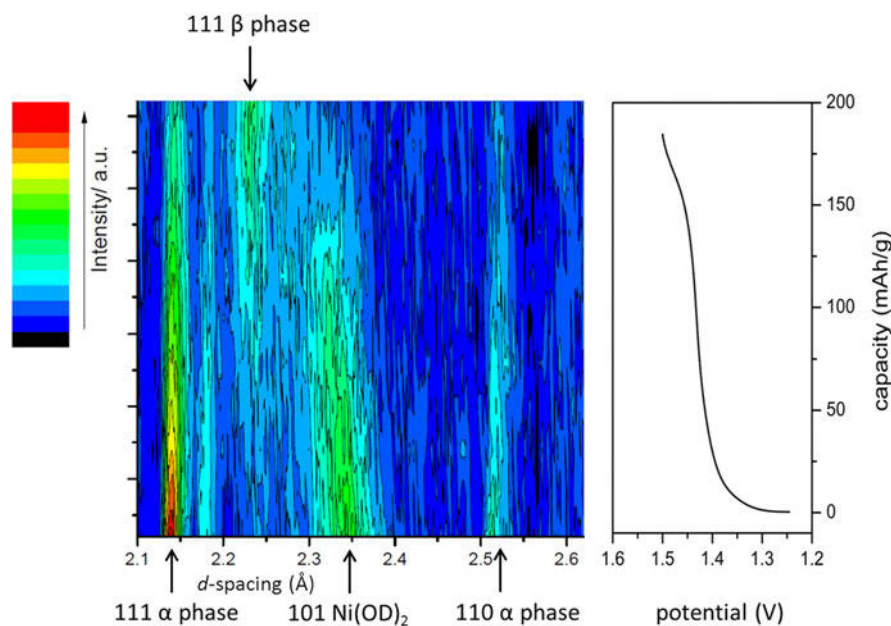


FIG. 2. Color map showing structural changes at both positive and negative electrodes in a Ni-MH battery as a function of charge and the voltage profile versus capacity for the cell measured in situ.

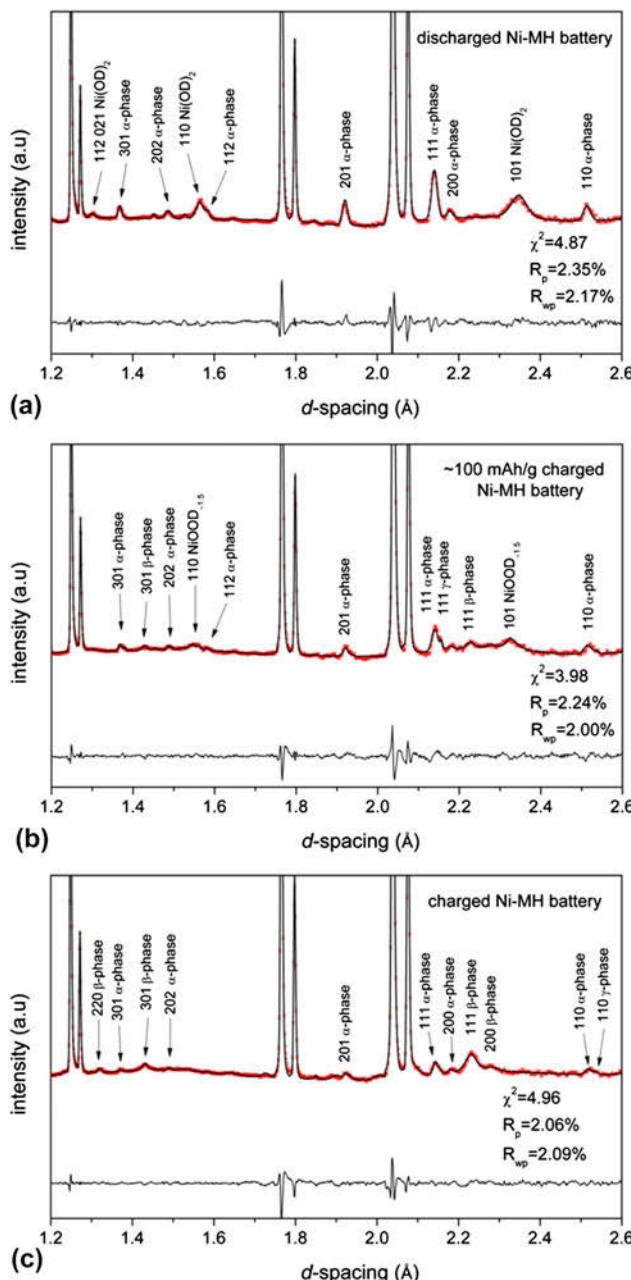


FIG. 3. Fitted neutron diffraction patterns of the cell loaded with a Ni-MH battery (a) discharged, (b) charged at 100 mA h/g, and (c) fully charged. Reflections of Ni(OD)₂ and LaNi₅-type alloy are marked and goodness-of-fit parameters presented for each fit.

not be obtained. All data banks were carefully investigated in the search of “new” reflections corresponding to a non-isostructural charged β -NiOOD phase^{9,12} or to detect 110 and 101 reflections from the isostructural β -NiOOD phase which are expected to be strong in intensity.⁷ None of these were observed. It is clear, therefore, that the charged phase has low crystallinity (amorphous) and from this in situ experiment no structural information was obtained for the β -NiOOD phase.

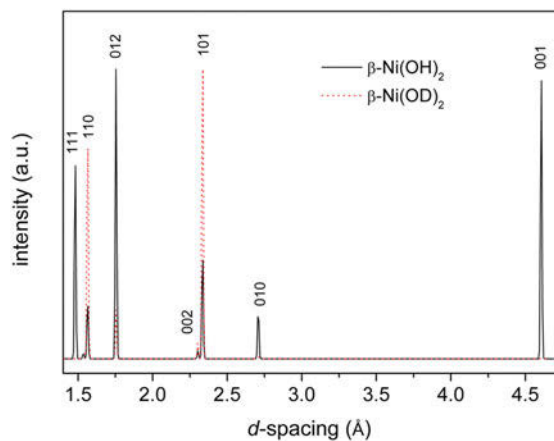


FIG. 4. Simulated neutron diffraction pattern of defect free β -Ni(OH)₂ (black trace) and β -Ni(OD)₂ (red trace) using CrystalMaker.⁴¹

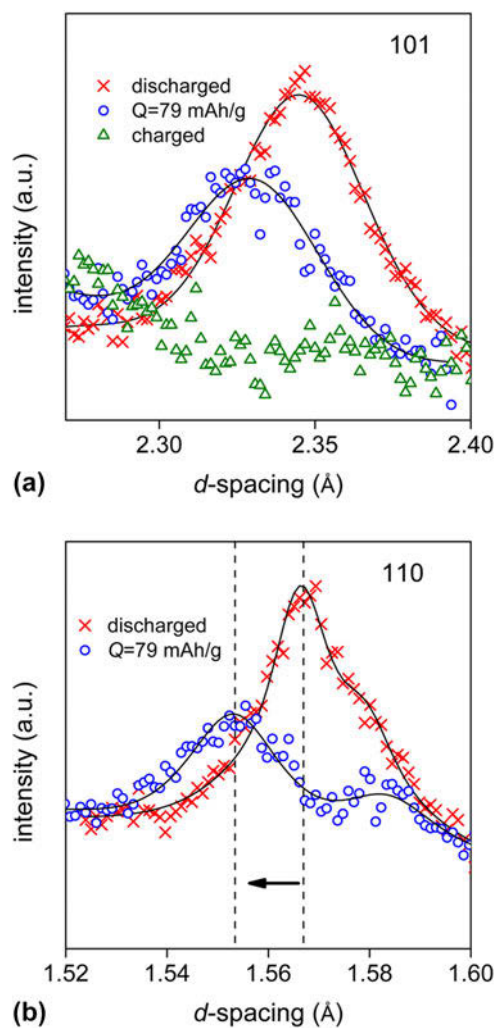


FIG. 5. Neutron diffraction data of the cell showing a) 101 and b) 110 reflections of Ni(OD)₂ at different charge states.

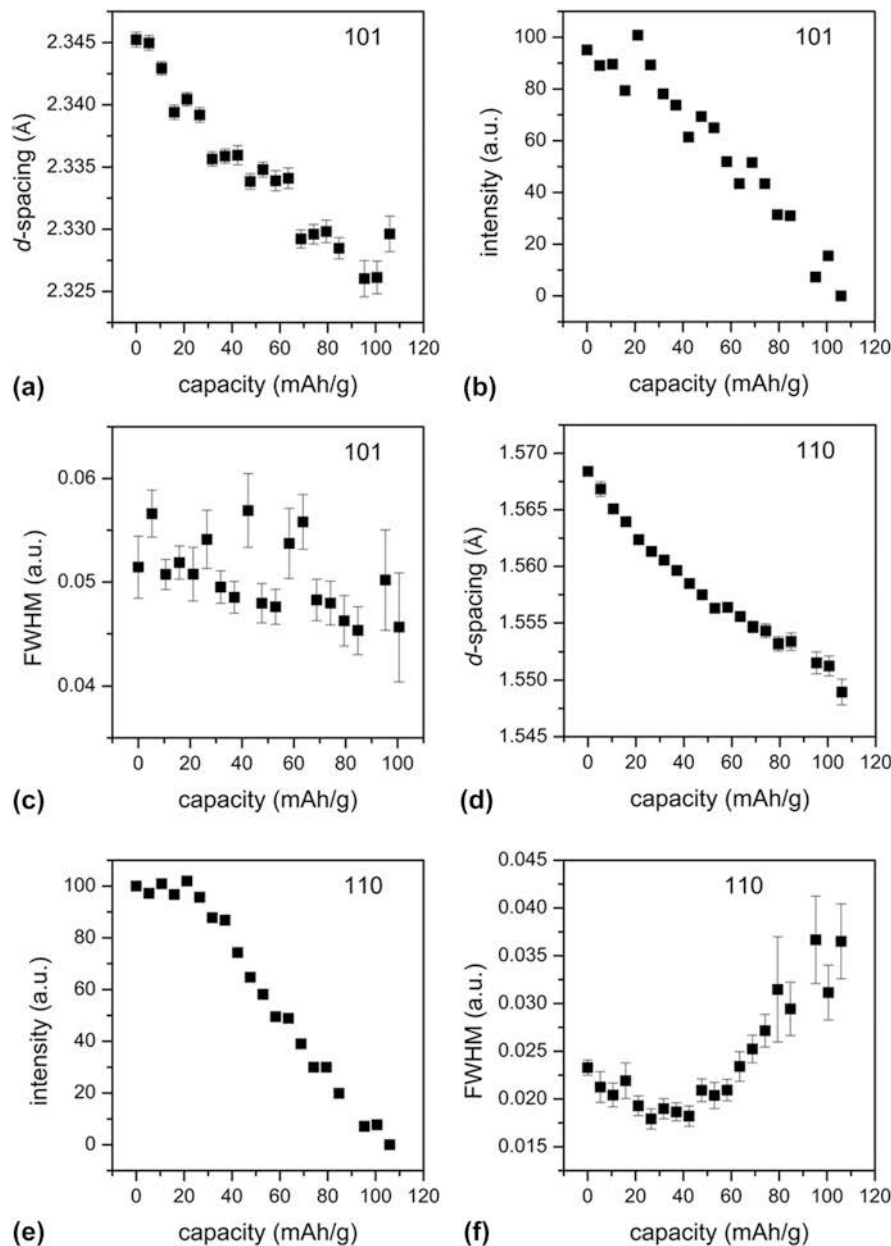


FIG. 6. Fitted parameters of Ni(OD)₂ as a function of battery capacity: a) *d*-spacing, b) intensity, and c) FWHM for the 101 reflection; d) *d*-spacing, e) intensity, and f) FWHM for the 110 reflection.

It is interesting to study, however, the behavior of the β_{II} -Ni(OD)₂ on charge up to ~ 100 mA h/g. As expected, contraction of the *ab*-plane of the hexagonal unit cell occurs as the electrode is oxidized, but this takes place in the form of a solid solution regime. Until now, it has been generally assumed that charging of the β_{II} -Ni(OD)₂ phase proceeds as a biphasic reaction as mentioned in the introduction section and, if a solid solution region exists, this tends to be very narrow.⁴⁴ In this experiment we observe that the largest amount of deuterium contained at the positive electrode is de-intercalated from the electrode with no phase transformation involved up to ~ 100 mA h/g.

To gain more information from the positive electrode on charge, the formula⁴⁵ that relates *d*-spacing with lattice parameter shown below was used to extrapolate the behavior of the *c* axis and this is presented in Fig. 7.

$$\frac{1}{d^2} = \frac{4}{3} \left(\frac{h^2 + hk + k^2}{a^2} \right) + \frac{l^2}{c^2} \quad . \quad (1)$$

The *c* axis does not show a trend as observed for the 110 reflection on charge up to ~ 100 mA h/g, and this indicates that the solid solution regime only affects the *ab*-plane of the hexagonal unit cell. Any structural

change that occurs at the electrode for >100 mA h/g must involve variation of the *c* axis i.e., either being an isostructural or a nonisostructural phase transition.

With reference to the FWHM of reflections 101 and 110 of β_{II} -Ni(OH) as a function of charge, Figs. 6(c) and 6(f), respectively, two different behaviors are observed. The FWHM for the 101 reflection is particularly broad, as seen in Fig. 5(a), and it does not show a clear trend as the battery is charged, Fig. 6(c). However, the 110 reflection does show a trend which involves the peak becoming much broader, Fig. 6(f). The width of the 101 peak has been related to the amount of stacking faults in the hexagonal close packing of the oxygen atoms⁴² which, for the data range presented, remains unaffected. This indicates that disorder along the *c* axis is not increased during battery charge i.e., formation of stacking faults within the structure. The width of the 110 peak has been discussed in Ref. 7 as a lack of structural long range order interpreted as a collapse of the domains that build up the particles i.e., NiO₂ slabs adopt a mosaic-like structure on nickel oxidation.

B. Charge in situ studies of LaNi₅-type alloy

More diffraction peaks corresponding to the negative electrode were observed in neutron diffraction patterns collected in situ, Fig. 3(a), which allowed us to refine the crystal structure by the Rietveld method. Structural changes for this electrode were substantial as a function of charge, Figs. 2 and 3. In the discharged state Fig. 3(a), all peaks corresponding to the intermetallic compound or α phase were fitted using the structural model based on the CaCu₅-type structure in which the distribution of metallic atoms between the available sites 1*a*, 2*c*, and 3*g* has been previously reported.^{23,26} For each new phase that appeared in the diffraction pattern as a result of the charge process, profile values were refined using function 3 (Ref. 40) in GSAS as described in the

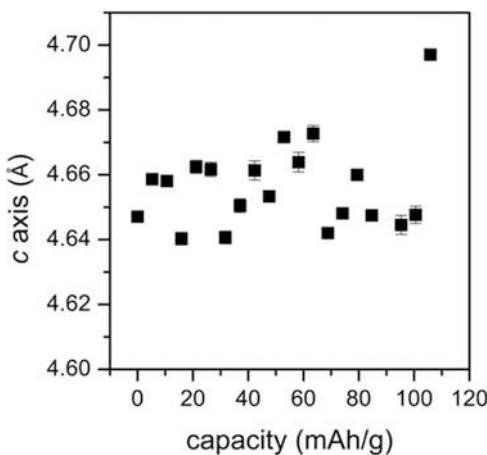


FIG. 7. *c* axis variation of Ni(OH)₂ as a function of battery capacity.

experimental section until good agreement was achieved and then fixed.

Initial refinements for the α -phase were not completely satisfactory even though attempts to use other profile functions were tested i.e., anisotropic line broadening. It was decided, therefore, to add some of the consecutive runs and investigate the fits using data of improved statistical quality. Figure 8 shows the merged data and the fits using the α phase (upper) and the fit when an extra phase was added into the refinement (lower). The latter accounts for the shoulder observed in the 111 reflection of the α phase and, in addition, fits all the corresponding intensities observed at higher *d*-spacings with respect to the α phase in the neutron diffraction patterns. Refined unit cell parameters using the CaCu₅-type structural model were slightly larger than in the α phase and this phase was referred to as γ .³⁰ On further charge, characteristic reflections of the β phase appeared in the neutron diffraction data. Therefore, three phases take part in the charge reaction process of the MmNi_{3.6}Al_{0.4}Mn_{0.3}Co_{0.7} electrode; α , γ , and β . The volume variation and phase fractions for the three phases as obtained from the structures refined using the in situ neutron diffraction data are shown in Fig. 9. During the first 8 h of the charge, the amount of α phase decreases whereas the hydride γ phase appears. Both phases show nearly constant unit cell volumes i.e., ~89 Å³ for α and ~91 Å³ for γ . The amount of γ phase reaches its maximum of ~25 wt%

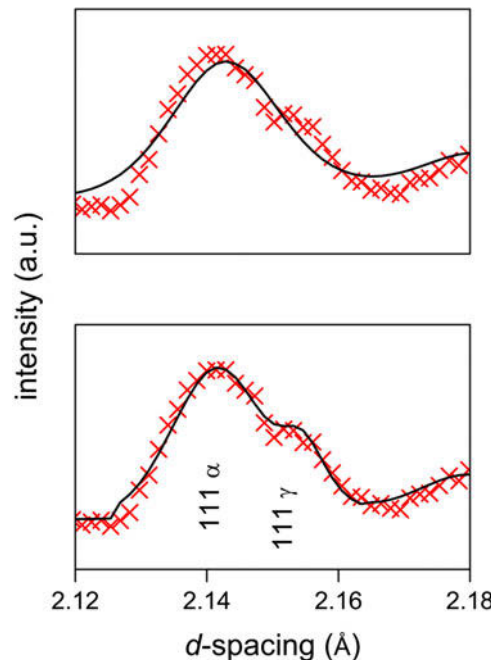


FIG. 8. In situ neutron diffraction data collected at ~90 mA h/g and fitted using a structural model with one phase or α (above) and two phases; α and γ (below).

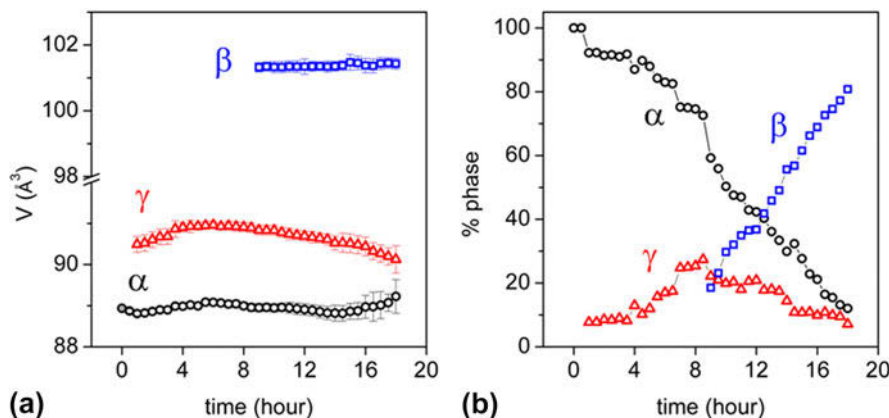


FIG. 9. Rietveld refinement results for the negative electrode as a function of time ($I = \sim 12$ mA); volume and phase fraction variation of the α -phase and hydride γ , β phases.

after 8 h of charge and then it decreases down to ~ 8 wt% at the end of charge. In the meantime, the β phase appears when the γ phase wt% is maximum and from that point increases until it reaches nearly 80 wt% of the electrode weight. The refined cell volume for the β phase also remains constant. The above results indicate that the charge process only involves phase transformations and no evidence of solid solution behavior was observed. Similar studies using an intermetallic compound of very close stoichiometry $MmNi_{3.61}Al_{0.39}Mn_{0.3}Co_{0.69}$ (Ref. 30) reported first the coexistence of two hydride phases; γ and β , and refined wt% for each phase as a function of charge agree well with our results. The presence of the intermediate γ phase was discussed in terms of thermodynamic equilibrium comparing results to solid–gas measurements and it was concluded that the γ phase was metastable during the charge process which was conducted at faster rates than in our experiment (C/18). Investigation of the charge/discharge reaction taking place at the negative electrode is of paramount importance because it has been shown that the main limitation of the Ni-MH battery life is linked to the degradation of this electrode.⁴⁶ After certain cycle life, the negative electrode suffers corrosion which, in turn, is governed by the type of reaction occurring at the electrode during cycling. The typical phase transition $\alpha \rightarrow \beta$ observed in various intermetallic compounds induces strain within the grains leading to the formation of fresh surfaces in contact with the electrolyte and increasing corrosion. The presence of an intermediate phase reduces the decrepitation process as observed in Ref. 30 and a reduction of corrosion level is expected at the electrode.

IV. CONCLUSIONS

In situ neutron diffraction measurements of a Ni-MH battery using commercially available electrodes have shown that important structural changes occur at both

electrodes as a function of charge. Ex situ cycling of the cell prior to in situ experiment successfully exchanged hydrogen by deuterium for the β_{II} -Ni(OH)₂ electrode while preserving the good electrochemical properties that characterize commercially available powders. Although only two peaks i.e., 101 and 110 from the β_{II} -Ni(OD)₂ positive electrode material were observed in the neutron diffraction patterns collected in situ, it was still possible to extract significant structural information. During electrode oxidation, there is a solid solution domain which, for the type of electrode investigated i.e., spherical microstructure of diameter < 10 μm and relevant concentration of stacking faults on the structure, is very large ($Q \leq 100$ mA h/g). No evidence of a charged $\sim Ni^{3+}$ phase has been observed and this was attributed to its low crystallinity or electrode amorphization during charge. In fact, direct evidence of the increase of disorder in the *ab* plane in the hexagonal unit cell has been detected based on the variation of the 110 peak width as a function of charge. The *c* axis of the β_{II} -Ni(OD)₂ phase remains unaffected for $Q \leq 100$ mA h/g. Overall, we would like to point out that the better electrochemical performance that commercial powders offer in comparison to crystalline materials may be related to an increase of disorder in the structure as well as the large solid solution regime observed during our experiments using in situ neutron powder diffraction.

The Rietveld method was used to obtain structural information on the negative electrode or α -phase of composition $MmNi_{3.6}Al_{0.4}Mn_{0.3}Co_{0.7}$, where $Mm = 50\text{--}55\%$ La, 30–35% Ce, 9–13% Nd, and 3–5% Pr during charge. The reaction involves transformations between the α -phase and two hydride phases; γ and β . All phases show characteristic reflections corresponding to a CaCu₅-type structure. The γ structure was difficult to study in detail because of a) its low wt% and b) similar unit cell dimensions to the α -phase. The appearance of an intermediate phase between α and β during charge has been discussed.

ACKNOWLEDGMENTS

We would like to thank Richard Haynes and Gavin Stenning for the help given during the in situ experiment and XRD data collection, respectively. Support from the Swedish Energy Agency is also acknowledged.

REFERENCES

- U. Köhler, C. Antonius, and P. Bäuerlein: Advances in alkaline batteries. *J. Power Sources* **127**, 45–52 (2004).
- M. Zolot, A.A. Pesaran, and M. Mihalic: Thermal evaluation of Toyota Prius battery pack. National Renewable Energy Laboratory internal document, 2002-01-1962.
- Inorganic Crystal Structure Database, <http://cds.dl.ac.uk>.
- C. Daniel and J.O. Besenhard, editors. *Handbook of Battery Materials*, 2nd ed. (Wiley-VCH, Germany, 2011).
- H. Bode, K. Dehmelt, and J. Witte: Zur kenntnis der nickelhydroxidelektrode-I. Über das nickel (II)-hydroxidhydrat. *Electrochim. Acta* **11**, 1079–1087 (1966).
- D. Tuomi: The forming process in nickel positive electrodes. *J. Electrochem. Soc.* **112**(1), 1–12 (1965).
- L. Eriksson, U. Palmqvist, H. Rundlof, U. Thuresson, and R. Sjovall: Structural aspects on the charged positive Ni electrode. *J. Power Sources* **107**, 34–41 (2002).
- G.W.D. Briggs and W.F.K. Wynne-Jones: The nickel oxide electrode (Part 3). *Trans. Faraday Soc.* **52**, 1272–1281 (1956).
- M. Casas-Cabanas, J. Canales-Vazquez, J. Rodriguez-Carvajal, and M.R. Palacin: Deciphering the structural transformations during nickel oxyhydroxide electrode operation. *J. Am. Chem. Soc.* **129**(18), 5840–5842 (2007).
- M. Casas-Cabanas, J. Canales-Vazquez, J. Rodriguez-Carvajal, and M.R. Palacin: Characterizing nickel battery materials: Crystal structure of β -NiOOH. *Mater. Res. Symp. Proc.* **1126**, 131–136 (2009).
- A. Van der Ven, D. Morgan, Y.S. Meng, and G. Ceder: Phase stability of nickel hydroxides and oxyhydroxides. *J. Electrochem. Soc.* **153**(2), A210–A215 (2006).
- V.Yu. Kazimirov, M.B. Smirnov, L. Bourgeois, L. Guerlou-Demourgues, L. Servant, A.M. Balagurov, I. Natkaniec, N.R. Khasanova, and E.V. Antipov: Lattice dynamics of Ni and Mg hydroxides. *Solid State Ionics* **181** (39–40), 1764–1774 (2010).
- P. Oliva, J. Leonardi, J.F. Laurent, C. Delmas, J.J. Braconnier, M. Figlarz, F. Fievet, and A. Guibert: Review of the structure and the electrochemistry of nickel hydroxides and oxy-hydroxides. *J. Power Sources* **8**(2), 229–255 (1982).
- R.S. McEwen: Crystallographic studies on nickel hydroxide and their higher nickel oxides. *J. Phys. Chem.* **75**(12), 1782–1789 (1971).
- M. Butel, L. Gautier, and C. Dalmas: Cobalt oxyhydroxides obtained by ‘chimie douce’ reactions: Structure and electronic conductivity properties. *Solid State Ionics* **122**, 271–284 (1999).
- W-K. Hu, X-P. Gao, D. Noréus, T. Burchardt, and N.K. Nakstad: Evaluation of nano-crystal sized α -nickel hydroxide as an electrode material for alkaline rechargeable cells. *J. Power Sources* **160**, 704–710 (2006).
- A.B. Béléké, E. Higuchi, H. Inoue, and M. Mizuhata: Durability of nickel-metal hydride (Ni-MH) battery cathode using nickel-aluminum layered double hydroxide/carbon (Ni-Al LDH/C) composite. *J. Power Sources* **247**, 572–578 (2014).
- X. Zhao and L. Ma: Recent progress in hydrogen storage alloys for nickel/metal hydride secondary batteries. *Int. J. Hydrogen Energy* **34**, 4788–4796 (2009).
- X. Zhou, K. Young, J. West, J. Regalado, and K. Cherisol: Degradation mechanisms of high-energy bipolar nickel metal hydride battery with AB₅ and A₂B₇ alloys. *J. Alloys Compd.* **580**, S373–S377 (2013).
- S. Yasuoka, Y. Magari, T. Murata, T. Tanaka, J. Ishida, H. Nakamura, T. Nohma, M. Kihara, Y. Baba, and H. Teraoka: Development of high-capacity nickel-metal hydride batteries using superlattice hydrogen-absorbing alloys. *J. Power Sources* **156**, 662–666 (2006).
- Z. Ye, D. Noréus, and J.R. Howlett, III: Metal hydrides for high-power batteries. *Mater. Res. Bull.* **38**(6), 504–508 (2013).
- M. Latroche, J-M. Joubert, A. Percheron-Guégan, and F. Bourée-Vigneron: Neutron diffraction study of the deuterides of the over-stoichiometric compounds LaNi_{5+x}. *J. Solid State Chem.* **177**(4–5), 1219–1229 (2004).
- J-M. Joubert, R. Cerný, M. Latroche, A. Percheron-Guégan, and K. Yvon: Site occupancies in the battery electrode material LaNi_{3.55}Mn_{0.4}Al_{0.3}Co_{0.75} as determined by multiwavelength synchrotron powder diffraction. *J. Appl. Crystallogr.* **31**, 327–332 (1998).
- C. Lartigue, A. Percheron-Guégan, J.C. Achard, and J.L. Soubeyroux: Hydrogen (deuterium) ordering in the β -LaNi₅D_{x>5} phases: A neutron diffraction study. *J. Less Common Met.* **113**, 127–148 (1985).
- A. Percheron-Guégan, C. Lartigue, J.C. Achard, P. Germi, and F. Tasset: Neutron and x-ray diffraction profile analyses and structure of LaNi₅, LaNi_{5-x}Al_x and LaNi_{5-x}Mn_x intermetallics and their hydrides (deuterides). *J. Less Common Met.* **74**(1), 1–12 (1980).
- J.J. Biendicho, M. Roberts, C. Offer, D. Noreus, E. Widenkvist, R.I. Smith, G. Svensson, K. Edstrom, S.T. Norberg, and S. Hull: New in situ neutron diffraction cell for electrode materials. *J. Power Sources* **248**, 900–904 (2014).
- M. Latroche, A. Percheron-Guégan, Y. Chabre, C. Poinsignon, and J. Pannetier: In situ neutron diffraction study of the behaviour of LaNi_{4.5}Al_{0.5}D_x electrode during deuterium charge-discharge. *J. Alloys Compd.* **189**, 59–65 (1992).
- M. Latroche, J. Rodríguez-Carvajal, A. Percheron-Guégan, and F. Bourée-Vigneron: Structural studies of LaNi₄CoD_{6.11} and LaNi_{3.55}Mn_{0.4}Al_{0.3}Co_{0.75}D_{5.57} by means of neutron powder diffraction. *J. Alloys Compd.* **218**, 64–72 (1995).
- M. Latroche, A. Percheron-Guégan, and F. Bourée-Vigneron: Investigation of the crystallographic structures of LaNi₄CoD_{4.4} and LaNi_{3.55}Mn_{0.4}Al_{0.3}Co_{0.75}D_x (x=2.0 and 4.6 D/f.u.) by neutron powder diffraction. *J. Alloys Compd.* **265**, 209–214 (1998).
- M. Latroche, A. Percheron-Guégan, and Y. Chabre: Influence of cobalt in MnNi_{4.3-x}Mn_{0.3}Al_{0.4}Co_x alloy (x=0.36 and 0.69) on its electrochemical behaviour studied by in situ neutron diffraction. *J. Alloys Compd.* **293–295**, 637–642 (1999).
- M. Latroche, Y. Chabre, B. Decamps, A. Percheron-Guégan, and D. Noréus: In situ neutron diffraction study of the kinetics of metallic hydride electrodes. *J. Alloys Compd.* **334**, 267–276 (2002).
- M. Latroche, A. Percheron-Guégan, Y. Chabre, J. Bouet, J. Pannetier, and E. Ressouche: Intrinsic behaviour analysis of substituted LaNi₅-type electrodes by means of in situ neutron diffraction. *J. Alloys Compd.* **231**(1–2), 537–545 (1995).
- J. Schefer, L. Keller, Y. Zannatul, S. Paofai, M. Schmalz, M. Krebs, M. Ceretti, and W. Paulus: Electrochemical reduction of La(Ni_{3.6}Co_{0.7}Al_{0.4}Mn_{0.3}) (LAMM) deuterides investigated by in situ neutron powder diffraction: Following the metal-hydride phase transition under technical operating conditions in a KOD electrolyte. *Int. J. Hydrogen Energy* **38**(14), 5903–5910 (2013).
- W. Peng, L. Redey, A.N. Jansen, D.R. Vissers, K.M. Myles, J.M. Carpenter, J.W. Richardson, G.L. Burr, and J.R. Selman: Electrochemical and in situ neutron diffraction investigations of La-Ni-Al-H alloys. *J. Electrochem. Soc.* **144**(11), 3836–3844 (1997).

35. W.K. Pang, V.K. Peterson, N. Sharma, J-J. Shiu, and S-H. Wu: Lithium migration in Li₄Ti₅O₁₂ studied using in situ neutron powder diffraction. *Chem. Mater.* **26**(7), 2318–2326 (2014).
36. M. Roberts, J.J. Biendicho, S. Hull, P. Beran, T. Gustafsson, G. Svensson, and K. Edstrom: Design of a new lithium ion battery test cell for in situ neutron diffraction measurements. *J. Power Sources* **226**, 249–255 (2013).
37. M. Bianchini, J.B. Leriche, J-L. Laborier, L. Gendrin, E. Suard, L. Croguennec, and C. Masquelier: A new null matrix electrochemical cell for Rietveld refinements of in-situ or operando neutron powder diffraction data. *J. Electrochem. Soc.* **160**(11), A2176–A2183 (2013).
38. S. Hull, R.I. Smith, W.I.F. David, A.C. Hannon, J. Mayers, and R. Cywinski: The Polaris powder diffractometer at ISIS. *Physica B* **180–181**, 1000–1002 (1992).
39. J. Rodriguez-Carvajal: Recent advances in magnetic structure determination by neutron powder diffraction. *Physica B* **192**, 55–69 (1993).
40. A.C. Larson and R.B. Von Dreele: *Report LA-UR-86-748* (Los Alamos National Laboratory, Los Alamos, NM87545, 1990).
41. D. Palmer: *CrystalMaker Software Version 2.2.3* (Crystal Maker Software Ltd., Oxford, England, 2009).
42. C. Delmas and C. Tessier: Stacking faults in the structure of nickel hydroxide: A rationale of its high electrochemical activity. *J. Mater. Chem.* **7**(8), 1439–1443 (1997).
43. E. Shangguan, Z. Chang, H. Tang, X-Z. Yuan, and H. Wang: Comparative structural and electrochemical study of high density spherical and non-spherical Ni(OH)₂ as cathode materials for Ni-metal hydride batteries. *J. Power Sources* **196**(18), 7797–7805 (2011).
44. F. Barbé, M.R. Palacin, Y. Chabre, O. Isnard, and J-M. Tarascon: In situ neutron powder diffraction of a nickel hydroxide electrode. *Chem. Mater.* **16**(20), 3936–3948 (2004).
45. T. Hahn: *International Tables for Crystallography, Vol. A: Space-Group Symmetry* (Reidel Publishing Company, Dordrecht, Netherlands, 2006).
46. C.S. Wang, M. Marrero-Cruz, J.H. Baricuatro, M.P. Soriaga, D. Serafini, and S. Srinivasan: Corrosion behaviour of AB₅-type hydride electrodes in alkaline electrolyte solution. *J. Appl. Electrochem.* **33**, 325–331 (2003).